GPS Solutions (2023) 27:69
https://doi.org/10.1007/s10291-023-01409-5

RESEARCH

Long-term performance analysis of BDS-3 precise point positioning (PPP-B2b) service

Shuang Sun[1] · Min Wang[1] · Changjian Liu[1] · Xin Meng[1] · Rui Ji[1]

Received: 14 October 2022 / Accepted: 27 January 2023 / Published online: 15 February 2023

Abstract

Since 2020, the BeiDou Navigation Satellite System (BDS) has launched new precise point positioning service which provides precise correction of GPS and BDS-3 satellites to help users realize real-time precise point positioning, known as PPP-B2b service. After being fully operational for more than one year, this contribution comprehensively analyzes the performance of PPP-B2b in terms of correction availability, clock and orbit quality and positioning accuracy with PPP-B2b messages of nearly 48 weeks from 2021 to 2022. The results show that in the PPP-B2b service, the orbit radial differences of BDS-3 MEO, GPS, and BDS-3 IGSO satellites are 0.056 m, 0.069 m, and 0.172 m, respectively, compared to the GFZ final orbit, while the difference of along-track and cross-track is more than three times the radial. For BDS-3 MEO satellites from different manufacturers, the RMS of Satellite Laser Ranging (SLR) residuals is different, with a maximum of 0.11 m. Restricted by the regional tracking network, the correction series of PPP-B2b service are discontinuous, and there are constant satellite-specific clock biases in different arcs of the satellite. Thus, the STD and RMS of satellite clock offset and signal-in-space ranging error (SISRE) are calculated using the method of weighting by arcs. The STD of SISRE for BDS-3 MEO, GPS and BDS-3 IGSO are 0.059 m, 0.092 m and 0.174 m, respectively. A total of 108 days of observation data from 12 MGEX stations of the East Asia region are selected to analyze the positioning performance of PPP-B2b. The results of day-by-day static PPP are stable at the centimeter level, while the average convergence time of GPS-only (61.65 min) is longer than BDS-3-only (45.12 min), which the constant bias in clock offset may cause. To analyze the effect of this bias, the bias is calculated and used as a correction to the PPP-B2b clocks. The convergence time of BDS-3 and GPS positioning is reduced by 48.7% and 65.9%, respectively, after correcting this bias, which confirms the influence of clock constant bias on positioning convergence.

Keywords PPP-B2b · Precise point positioning · SISRE · Constant satellite-specific bias

Introduction

Precise point positioning (PPP) is a technology that can achieve centimeter-level positioning accuracy with only one receiver (Malys and Jensen 1990; Zumberge et al. 1997). Precise orbit and clock offset of GNSS satellites are essential to the realization of PPP. To response the rapidly growing demand of real-time precise positioning, since 2013, the International GNSS Service (IGS) has launched real-time service (IGS-RTS) to broadcast real-time orbit and clock in Radio Technical Commission for Maritime Services (RTCM) protocol over Internet network (Montenbruck et al. 2017). Initially, IGS-RTS only provided real-time service for GPS and GLONASS, and early evaluations showed orbits and clocks are of centimeter-level accuracy for GPS and decimeter level for GLONASS (Hadas and Bosy

✉ Min Wang
different9@163.com

Shuang Sun
daben64ss@163.com

Changjian Liu
chxylcj@163.com

Xin Meng
18749491423@163.com

Rui Ji
JerryRV0213@163.com

[1] PLA Strategic Support Force Information Engineering University, Zhengzhou 450001, China

2014). With the development of the Global Navigation Satellite System (GNSS), IGS Analysis Centers (ACs), such as D'Etudes Spatiales (CNES), German Research Centre of Geosciences (GFZ), WuHan Unversity (WHU), and Center for Orbit Determination in Europe (CODE), have successively provided multi-system real-time services. Kazmierski et al. (2020) assessed the quality of CNES real-time products, with most satellites having an availability of more than 90% for GPS, Galileo, GLONASS and BDS, and overall the signal-in-space ranging error (SISRE) of all satellite systems being in the centimeter level, and users can obtain real-time positioning results at decimeter level using the service (Nie et al. 2019). Zhang et al. (2018) compared the real-time service performance of different ACs, and the results showed that the difference of GPS orbit and clock offset of different RTS services was at the centimeter level. Guo et al. (2022) demonstrated that the product quality of different analysis centers is comparable by real-time PPP time transfer results. However, for users with limited land-based communication supports or even out of reach of the network coverage, it may not be feasible for users to receive real-time GNSS orbit and clock corrections (Nie et al. 2020). Currently, some commercial companies offer satellite-based PPP services with a centimeter or decimeter-level positioning accuracy via satellite communications, but users have to pay for specialized receivers and usage costs (Leandro et al. 2011; Dai et al. 2016). In addition to the commercial services, some GNSS recently provide open satellite-based PPP services, such as Centimeter Level Augmentation Service (CLAS) of QZSS and Hight Accuracy Service (HAS) of Galileo, which greatly expanded the development and application of satellite-based PPP (Borio et al. 2020).

On July 31, 2020, the full constellation of the BDS-3 system was completed and provided global services. Among seven major services provided by BDS-3, the precise point positioning service (PPP-B2b) broadcasts the orbit and clock correction to China and its surrounding areas (75°E–135°E, 10°N–55°N) through the B2b signals of three GEO satellites, which is an alternative to realize precise positioning without additional network communication and cost (CSNO 2021a, b). Liu et al. (2020) described the signal design and implementation of PPP-B2b. Lu et al. (2021) used a software-defined receiver to decode and analyze the PPP-B2b correction and demonstrated the availability of the PPP-B2b in the service area. With the correction broadcast by PPP-B2b, the satellite clock accuracy can be significantly improved by about 85.1% (Xu et al. 2021). Preliminary positioning assessments show that PPP-B2b has better satellite availability in the service coverage compared to real-time products of CNES and WHU. (Tao et al. 2021; Liu et al. 2022). At present, PPP-B2b only provides the positioning correction for BDS-3 and GPS, and different strategies are adopted for two systems for estimating orbit and clock offset (Tang et al. 2022), leading to the difference of positioning capability (Ren et al. 2021; Zhang et al. 2022). The study by Tao et al. (2021) found that there was a satellite-related constant bias in the PPP-B2b clock offset, and the bias of GPS was larger than that of BDS-3, resulting in a positioning convergence time of GPS being longer than BDS-3. At the time of the above research, the PPP-B2b had just been launched for a limited period, and long-term analysis was not feasible. Nowadays, the PPP-B2b has been in service for more than one year, allowing us to analyze the performance of PPP-B2b with a long-term perspective and elaborate on some characteristics in detail.

The first part briefly introduces the evaluation methods of orbit and clock offset adopted in this contribution. In the second part, with the collection of PPP-B2b correction for nearly one year, the accuracy analysis of orbit, clock offset and SISRE of PPP-B2b service is carried out. Then the positioning experiment is carried out to analyze the positioning performance using more than 100 days of observations from 12 MGEX stations. Finally, the effect of the constant bias of the clock offset on the positioning results is analyzed, and some conclusions are summarized.

Methodology

At present, PPP-B2b messages contain four types of correction: the satellite mask, orbit correction, clock correction, and differential code bias (DCB) correction. And the correction refers to the CNAV1 navigation messages on the B1C signal of BDS-3 and LNAV navigation messages for GPS, respectively (CSNO 2020a, b). The BeiDou Navigation Satellite System Time (BDT) and the BeiDou Coordinate System (BDCS) are adopted as a time reference and coordinate reference, respectively. This section focuses on the evaluation method of the corrected PPP-B2b orbit and clock offset.

Orbit assessment method

The post-processing product generated by GFZ is used as a reference to assess the quality of the PPP-B2b orbit, and the difference in the reference frame of the two products is ignored. Note that the GFZ orbit takes the satellite center-of-mass (CoM) as the reference, while the PPP-B2b service orbit takes the antenna phase center (APC) as the reference point. Before comparison, the antenna phase center offset (PCO) should be corrected to convert the PPP-B2b reference point to the satellite CoM. The difference vector of satellite orbit in radial, along-track and cross-track directions can be calculated as follows:

$$[\,\delta R\ \delta A\ \delta C\,]^T = \boldsymbol{R}_2.(\boldsymbol{X}_{\mathrm{GFZ}} - (\boldsymbol{X}_{\mathrm{B2b}} + \boldsymbol{R}_1.\boldsymbol{V}_{\mathrm{PCO_{sys}}})) \tag{1}$$

$$\boldsymbol{V}_{\mathrm{PCO_G}} = \frac{f_1^2}{f_1^2 - f_2^2}\boldsymbol{V}_{L_1} - \frac{f_2^2}{f_1^2 - f_2^2}\boldsymbol{V}_{L_2} \tag{2}$$

$$\boldsymbol{V}_{\mathrm{PCO_C}} = \boldsymbol{V}_{B_3} \tag{3}$$

where $\boldsymbol{X}_{\mathrm{GFZ}}$ is the satellite position vector from GFZ, $\boldsymbol{X}_{\mathrm{B2b}}$ is the PPP-B2b orbit vector, and $\boldsymbol{V}_{\mathrm{PCO_{sys}}}$ is the PCO correction vector. Equations (2) and (3) are used to calculate the PCO correction for GPS and BDS-3, respectively. $\boldsymbol{V}_{L_1}$ and $\boldsymbol{V}_{L_2}$ are the PCO correction vector of L_1 and L_2 for GPS. $\boldsymbol{V}_{B_3}$ is the PCO correction vector of B_3 for BDS. $\boldsymbol{R}_2$ is the transformation matrix from Earth-Center-Earth-Fixed (ECEF) frame to the RAC directions of the orbit. $\boldsymbol{R}_1$ is the satellite attitude matrix. They can be represented by the following unit vector $\boldsymbol{R}_1 = [\,\boldsymbol{e}_x\ \boldsymbol{e}_y\ \boldsymbol{e}_z\,]^T$,$\boldsymbol{R}_2 = [\,\boldsymbol{e}_R\ \boldsymbol{e}_A\ \boldsymbol{e}_C\,]^T$, where $\boldsymbol{e}_x$, $\boldsymbol{e}_y$, $\boldsymbol{e}_z$ are the unit vectors of X,Y, Z axes of the satellite-body frames in ECEF and $\boldsymbol{e}_R$, $\boldsymbol{e}_A$, $\boldsymbol{e}_C$ are the unit vectors of RAC in ECEF, where $\boldsymbol{e}_z = \boldsymbol{e}_R$. Therefore, the PCO correction has the following effects on the final orbit comparison results:

$$\begin{aligned} {}^T &= \boldsymbol{R}_2.(\boldsymbol{X}_{\mathrm{GFZ}} - \boldsymbol{X}_{\mathrm{B2b}}) - \boldsymbol{R}_2.\boldsymbol{R}_1.\boldsymbol{V}_{\mathrm{PCO}} \\ &= \boldsymbol{R}_2.(\boldsymbol{X}_{\mathrm{GFZ}} - \boldsymbol{X}_{\mathrm{B2b}}) - \begin{bmatrix} 0 & 0 & 1 \\ \boldsymbol{e}_A^T.\boldsymbol{e}_x & \boldsymbol{e}_A^T.\boldsymbol{e}_y & 0 \\ \boldsymbol{e}_C^T.\boldsymbol{e}_x & \boldsymbol{e}_C^T.\boldsymbol{e}_x & 0 \end{bmatrix}.\boldsymbol{V}_{\mathrm{PCO}} \end{aligned} \tag{4}$$

If incorrect PCO correction information is used, the deviation of the satellite-body frames on the Z-axis will cause a constant influence on the radial direction of the orbit. We use the antenna phase model published by IGS correction file to correct GPS, and the PCO model published by China Satellite Navigation Office (CSNO) is used to correct BDS (Tang et al. 2022).

It should be noted that it is not always proper to update the GPS PCO values according to the satellite switch logged in IGS Antex file. For example, according to the antenna correction file igs14_2223.atx, the satellite type and antenna models of G14, G22, and G23 were changed in July 2020. However, after applying the PCO model according to the valid time logged in igs14_2223.atx (set as strategy 1) for evaluation, there is a systematic bias in the radial orbit of the three satellites; the systematic bias is significantly reduced when the satellite PCO model is assigned to the same PRNs before July 2020 (set as strategy 2) is used. Figure 1 shows the result of the radial comparison between the PPP-B2b orbit and GFZ orbit from day-of-year (DOY) 7 to 17 in 2022, and the upper and lower parts are the comparison results of strategy 1 and strategy 2, respectively. It can be seen that there are decimeter to meter level radial systematic deviations for G14 and G23 satellites using strategy 1. Table 1 lists the correction differences for the two strategies. The difference of the PCO corrections in the U direction (Z-axis direction of the satellite-based system) of G14, G22 and G23 satellites are 0.69 m, 0.45 m and 1.23 m, respectively, between the two strategies, which is basically consistent with the magnitude of the systematic bias in radial. Therefore, strategy 2 is adopted to correct the PCO of GPS for the orbit evaluation in this contribution.

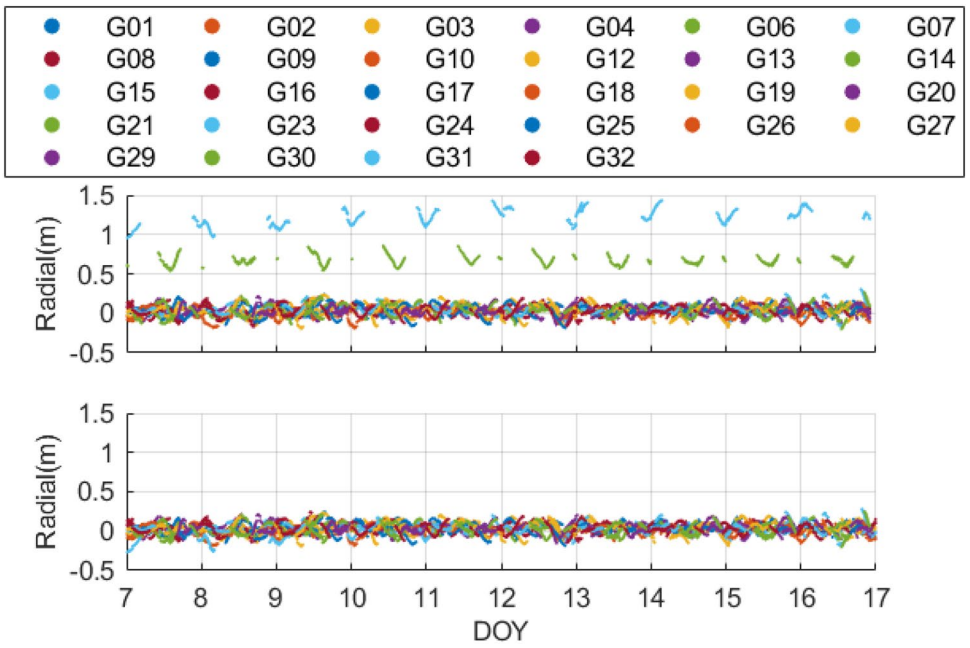

Fig. 1 GPS satellite radial orbit error for the two PCO models, the top and bottom parts are the results for strategy 1 and strategy 2, respectively

Table 1 PCO correction values for three satellites under two strategies

PRN	Strategy 1			Strategy 2		
	N (mm)	E (mm)	U (mm)	N (mm)	E (mm)	U (mm)
G14	4.9	−21.0	1991.9	−2.5	−1.7	1304.5
G22	−2.5	−1.7	1304.5	−2.2	2.2	850.6
G23	4.9	−21.0	1991.9	15.4	6.8	766.1

Clock offset assessment method

In order to set an absolute time reference in clock estimation, it is necessary to fix a receiver or satellite clock as the reference clock, which can cause a common bias for all clock offset. Meanwhile, due to the correlation between the ambiguity parameter and the clock offset in the carrier phase observations, pseudorange observations are needed to provide the absolute time reference, resulting in a satellite-specific bias in clock estimation for each satellite after the convergence of the ambiguity. Therefore, the clock offset can be expressed as follows (Guo et al. 2022):

$$\hat{t}^{s_i} = t_0 + t_0^{s_i} + \delta t^{s_i} \tag{5}$$

where t_0 is the bias due to the selection of the clock reference, which is identical for all satellites in the same epoch, $t_0^{s_i}$ is satellite-specific bias, and δt^{s_i} is the high-precision relative clock offset determined from the carrier phase observations.

When comparing products $\hat{t}_a^{s_i}$ and $\hat{t}_b^{s_i}$, the reference satellite is first selected to eliminate t_0 from the respective products by single-difference (SD) processing, and then the SD series of the different products are differenced from each other to obtain the double-difference (DD) series, which is used to evaluate the accuracy of the clock offset. The average clock offsets of the n visible satellites in the ephemeris are used as the reference clock to ensure the accuracy of the reference clock so that the DD clock series can be expressed as:

$$\begin{aligned}\nabla\Delta t_{a,b}^{s_i} &= t_a^{s_i} - t_b^{s_i} - \left(\frac{1}{n}\cdot\sum_{i=1}^{n} t_a^{s_i} - \frac{1}{n}\cdot\sum_{i=1}^{n} t_b^{s_i}\right) \\ &+ \delta t_a^{s_i} - \delta t_b^{s_i} - \left(\frac{1}{n}\cdot\sum_{i=1}^{n} \delta t_a^{s_i} - \frac{1}{n}\cdot\sum_{i=1}^{n} \delta t_b^{s_i}\right)\end{aligned} \tag{6}$$

for the PPP-B2b service, the differences in the satellites available for each epoch lead to differences in $\frac{1}{n}\cdot\sum_{i=1}^{n} t_a^{s_i}$ for different epochs, which can cause jumps in the DD series. The following equation is used as a constraint (Yao et al. 2017).

$$\sum_{i=1}^{M} \nabla\Delta t_{a,b}^{s_i}(k) = \sum_{i=1}^{M} \nabla\Delta t_{a,b}^{s_i}(k-1) \tag{7}$$

where M is the number of common satellites in the adjacent epoch, and the above equation is used to constrain the DD series on an epoch-by-epoch basis so that all epochs are unified with the first epoch.

The bias caused by the inconsistent reference signals of different products should also be eliminated. The reference signals of PPP-B2b for GPS and BDS-3 are L1/L2 IF combination and B3I, respectively, and the reference signals of GFZ products for the two systems are L1/L2 IF combination and B1/B3 IF combination. Before the comparison, the following equation was used to correct:

$$\hat{t}_{\mathrm{IF}_{B1B3}}^{s_i} = \hat{t}_{B3}^{s_i} - \frac{f_1^2}{f_1^2 - f_3^2} DCB_{B1B3}^{s_j} \tag{8}$$

where $\hat{t}_{\mathrm{IF}_{B1B3}}^{s_i}$ is the corrected clock offset, $f_1 = 1561.098$MHz and $f_3 = 1268.52$MHz are the B1 and B3 signal frequencies, respectively, and $DCB_{B1B3}^{s_j}$ is the satellite DCB correction.

Experiment and results analysis

The PPP-B2b messages collected by an experimental receiver from DOY 121 of 2021 to DOY 121 of 2022 are used for analysis in this contribution. During this period, some B2b messages are not collected for receiver relocation or software update.

Data availability analysis

Due to the characteristics of regional service, the PPP-B2b only has the correction of satellites visible around China. The availability of the corrections of PPP-B2b significantly influences the positioning performance. Figure 2 depicts the availability of the PPP-B2b from DOY 121 of 2021 to DOY 121 of 2022, in which there are B2b messages discontinuities due to receiver reasons from DOY 186–205, DOY 216–219, DOY 241–249 of 2021 and DOY 35–37 of 2022. The satellite availability ratio is derived by dividing the available time by the total time and is shown in Fig. 3. The G05 and G28 satellites do not have corrections after DOY 185 of 2021, which results in the availability below 5% in the experimental period. The availability ratio of the GPS and BDS-3 MEO satellites does not exceed 50%, except for

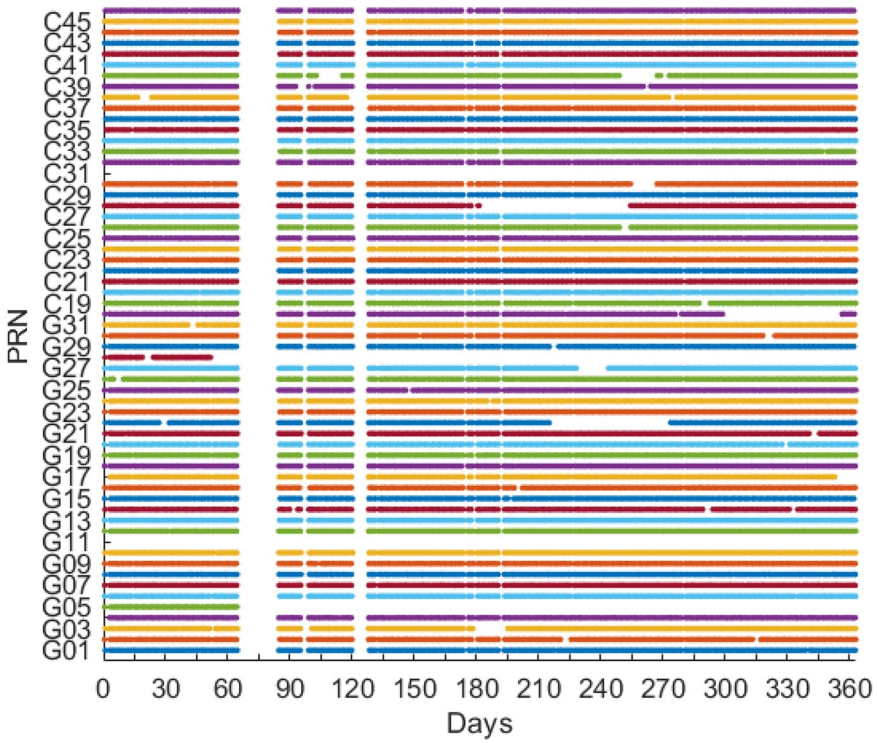

Fig. 2 Time distribution of available satellites for PPP-B2b service in the experimental period

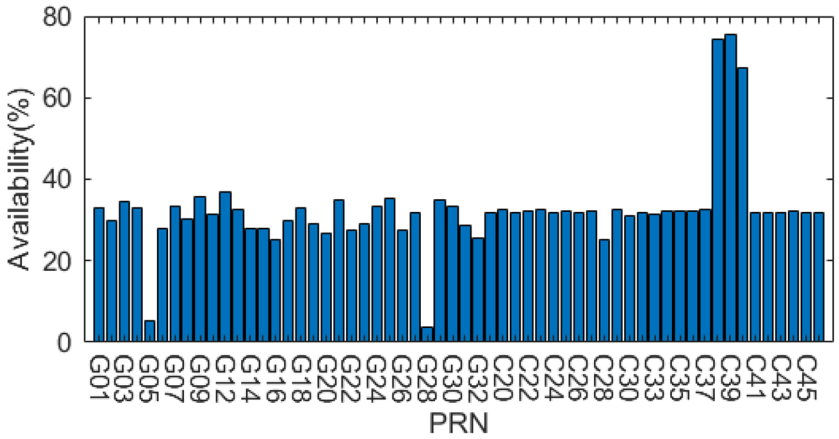

Fig. 3 Satellite availability during the experimental period

three BDS-3 IGSO satellites which are above 65%. However, it is still possible to guarantee the availability of more than 7 GPS satellites and more than 8 BDS-3 satellites at any one time.

Orbit assessment

By comparing the orbit of PPP-B2b and GFZ final product, Figs. 4, 5, and 6 show the orbit difference CDF (Cumulative Distribution Function) of BDS-3 MEO, GPS and BDS-3 IGSO satellites in radial, along-track, and cross-track directions, respectively. It can be seen that there are two trends in the radial CDF curve of the BDS-3 MEO satellite displayed in Fig. 4. The 90th-percentile of radial difference is 0.07 m and 0.12 m for satellites manufactured by China Aerospace Science and Technology Corporation (CAST) (except C45 and C46) and Shanghai Engineering Center for Microsatellites (SECM), respectively. This may be due to the quality of PCO calibrations provided by different manufacturers (Zajdel et al. 2022). Moreover, the 90th-percentile of radial difference is 0.12 m and 0.29 m for GPS and BDS-3 IGSO satellites, respectively.

In order to further assess the orbital quality of SECM and CAST satellites in PPP-B2b service, Satellite Laser Ranging (SLR) observations provided by the International Laser Ranging Service (ILRS) are used in this paper for ephemeris quality check. And the elimination threshold of SLR residuals is set to 1,000 mm. Figure 7 shows SLR

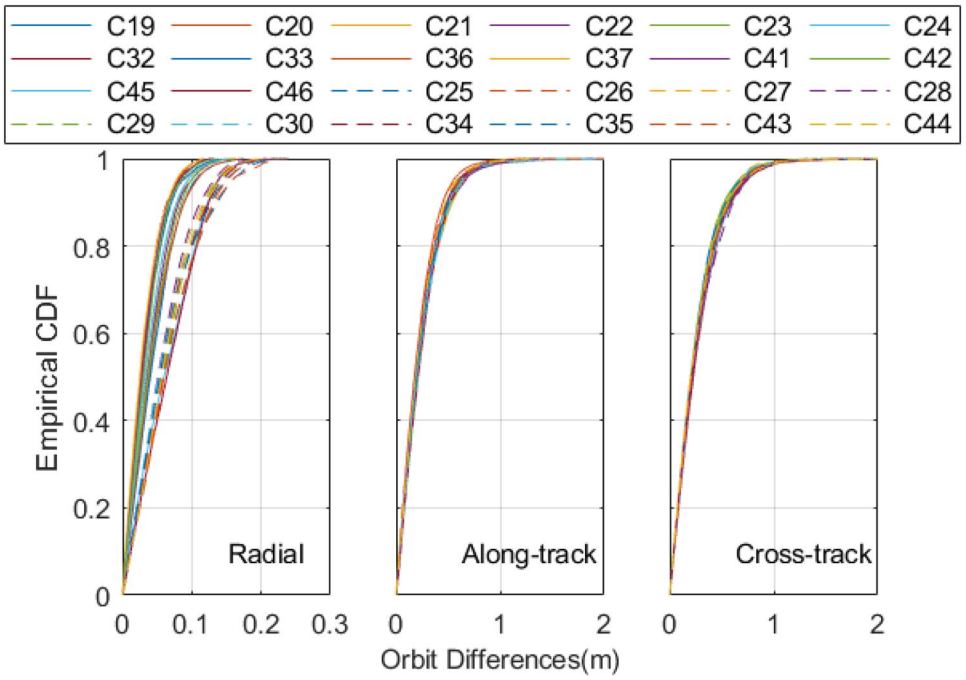

Fig. 4 BDS-3 MEO satellites orbit differences CDF of radial, along-track and cross-track directions. The solid lines represent the CAST satellites and the dotted lines represent the SECM satellites

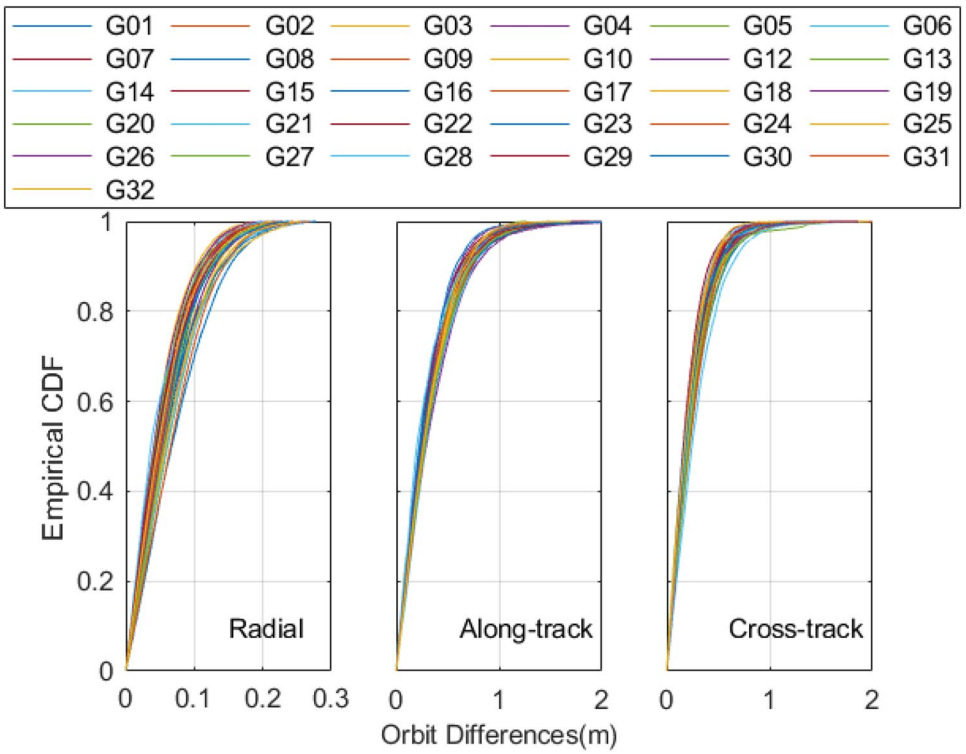

Fig. 5 GPS satellites orbit differences CDF of radial, along-track and cross-track directions

residuals of C20 (beidou3m2, C202), C21 (beidou3m3, C206), C29 (beidou3m9, C207) and C30 (beidou3m10, C208), in which the mean, STD, RMS, number of SLR data and number of eliminated anomalies are all shown in the figure. It can be seen that the RMS of C20 and C21 is smaller than that of C29 and C30, and the mean for the two types of satellites are opposite, which confirms the differences between different manufacturers (Sośnica et al. 2020).

Figure 8 shows the average orbit differences of the radial, along-track and cross-track directions of the BDS-3 satellite and the GPS satellite. Moreover, the orbit

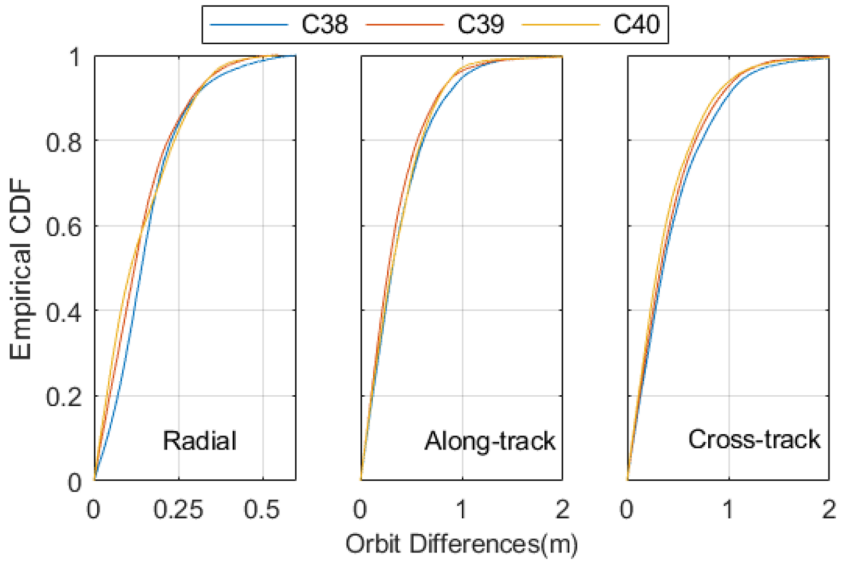

Fig. 6 BDS-3 IGSO satellites orbit differences CDF of radial, along-track and cross-track directions

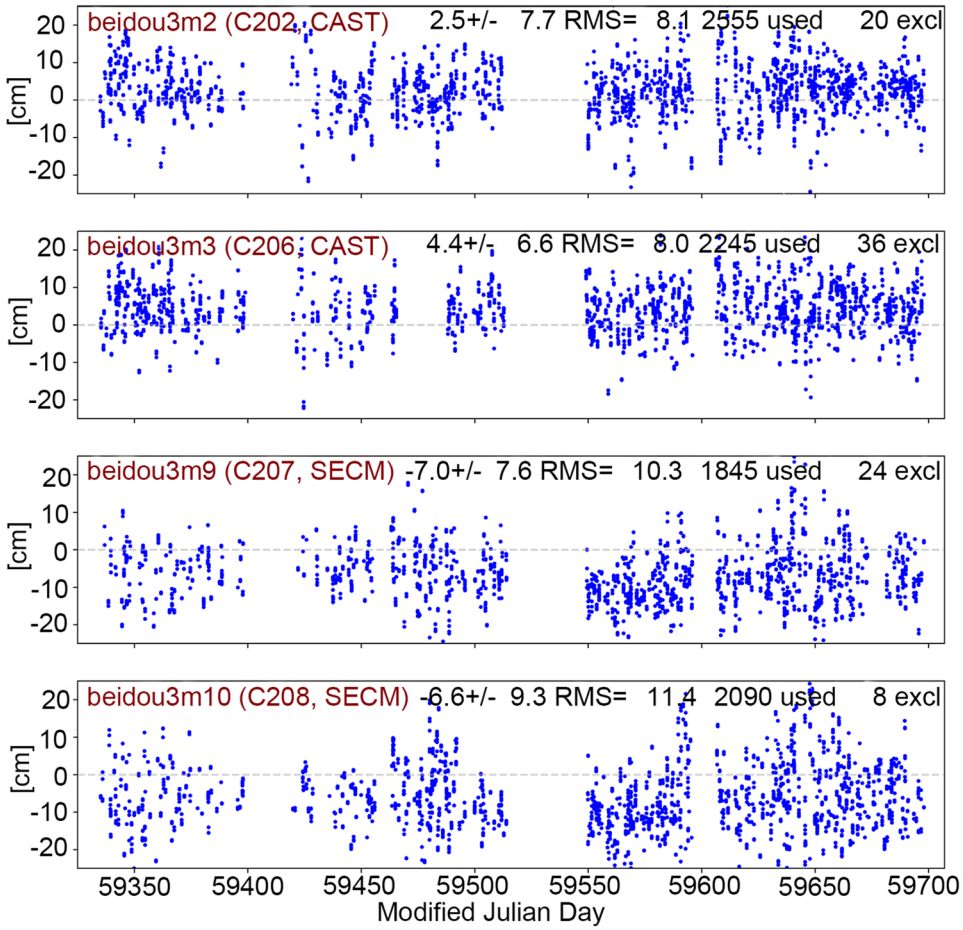

Fig. 7 SLR residuals of C20, C21, C29 and C30 from DOY 121 in 2021 to DOY 121 in 2022

differences of different satellites with the same type are similar. The root mean square (RMS) of orbit differences for BDS-3 MEO satellites are within 0.078 m, 0.325 m and 0.356 m in radial, along-track and cross-track directions, respectively, and within 0.086 m, 0.459 m and 0.362 m for GPS satellites. The cross-track error is smaller than the along-track error for the GPS satellites, while the opposite is true for the BDS-3 satellites. This may be due to the

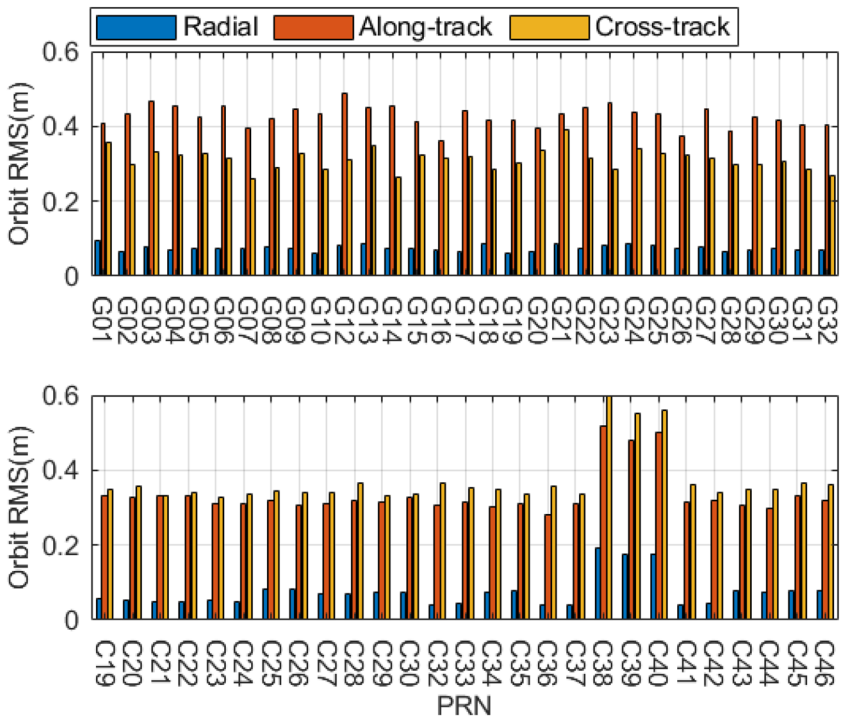

Fig. 8 RMS of the average orbit difference in radial, along-track and cross-track directions of each satellite in PPP-B2b service, and the upper and lower parts represent GPS and BDS-3, respectively

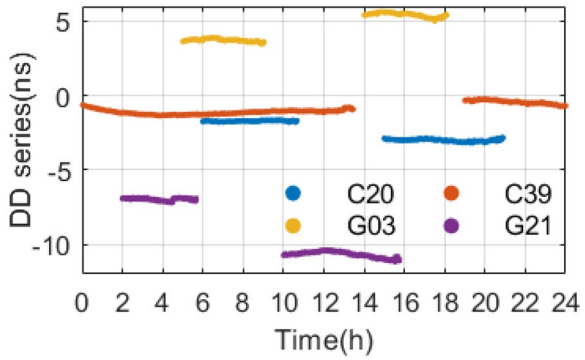

Fig. 9 DD series of C20, C39, G03 and G21 satellites on DOY 360 in 2021

influence of the observation value of BDS-3 Inter-Satellite Link (ISL) (Tang et al. 2018). Compared with GPS, the ISL measurements of BDS-3 have more contribution for the along-track component of orbit, which reduces the along-track error.

Clock accuracy assessment

To evaluate the accuracy of clock offset, the standard deviation (STD) of the DD series was calculated day-by-day and analyzed. Figure 9 shows a partial DD series of DOY 360 in 2021, for which two consecutive arcs exist for each of the four satellites. Although the DD series can be aligned with the above method, there are still jumps in different arcs, probably due to the influence of the accuracy of the pseudorange observations at the beginning of each arc segment, resulting in different arc segments $t_0^{s_i}$.

Table 2 lists the RMS and STD of the two arcs of the DD series of the four satellites. The arc length weights the results of the two arcs to obtain the average value. It can be found that the DD series of the four satellites on that day is relatively stable within each arc, and the STD is within 0.2 ns. However, the RMS is larger than STD and differs between different arcs, meaning that there is constant bias in the clock offset that varies with the arc. Despite this phenomenon, the constant bias in the clock offset will be absorbed by the ambiguity parameter and therefore have no effect on

Table 2 STD and RMS of DD series of each arc of four satellites

PRN	Segment1		Segment2		Mean	
	RMS (ns)	STD (ns)	RMS (ns)	STD (ns)	RMS (ns)	STD (ns)
C20	1.71	0.03	3.01	0.07	2.43	0.05
C39	1.13	0.15	0.46	0.13	0.95	0.14
G03	3.73	0.08	5.43	0.14	4.59	0.12
G21	6.97	0.08	10.68	0.20	9.26	0.15

the positioning result of PPP. Therefore, it is reasonable to calculate the STD of each satellite arc separately and weight the average to reflect the accuracy of the clock offset.

Figures 10 and 11 show the CDF of the daily clock offset STD for GPS and BDS-3 satellites. It can be seen that the CDF curves for the BD3-3 IGSO satellites (C38, C39 and C40) differ significantly from the MEO satellites, and the clock accuracy is significantly lower than that of the MEO satellites. For the BDS-3 MEO satellites, satellite C35 has the smallest CDF value, with the 95th percentile of STD being 0.38 ns. For GPS, the CDF curve of satellite G05 is stepped due to the shorter available time. Except for satellite G05, satellite G23 has the smallest CDF value, with the 95th percentile of STD being 0.5 ns.

Figure 12 shows the average STD and RMS of the clock DD series for each satellite during the experimental period. The STD of GPS clock offsets is within 0.25 ns for all satellites except G05 and G28, with an average STD of 0.20 ns, and the STD of BDS-3 MEO clock offset is within 0.2 ns, with an average STD of 0.16 ns. Although the RMS is the result of averaging across satellite arcs, it can be seen that the large constant bias in the PPP-B2b product results in a nanosecond-level RMS for the DD series, which is significantly higher than STD. Although this does not affect the final PPP positioning accuracy, it can significantly affect the PPP convergence time and the impact of this bias will be discussed later.

SISRE assessment

Montenbruck et al. (2014, 2018) provided the calculation of SISRE. For PPP-B2b, the evaluation method of weighting by arc length is used to calculate the STD and RMS values of the SISRE. The top and bottom panels of Fig. 13 show

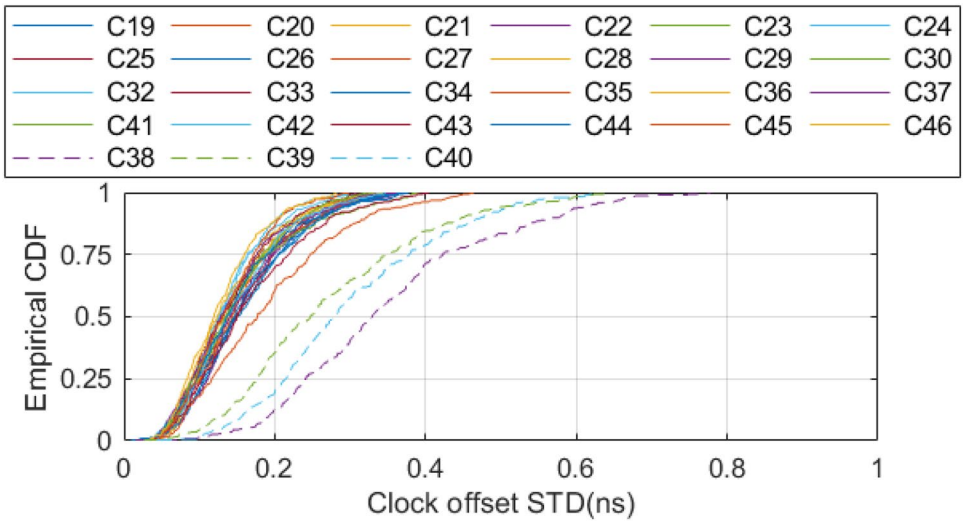

Fig. 10 CDF of BDS-3 satellite clock offset STD. The solid lines represent the MEO satellites and the dotted lines represent IGSO satellites

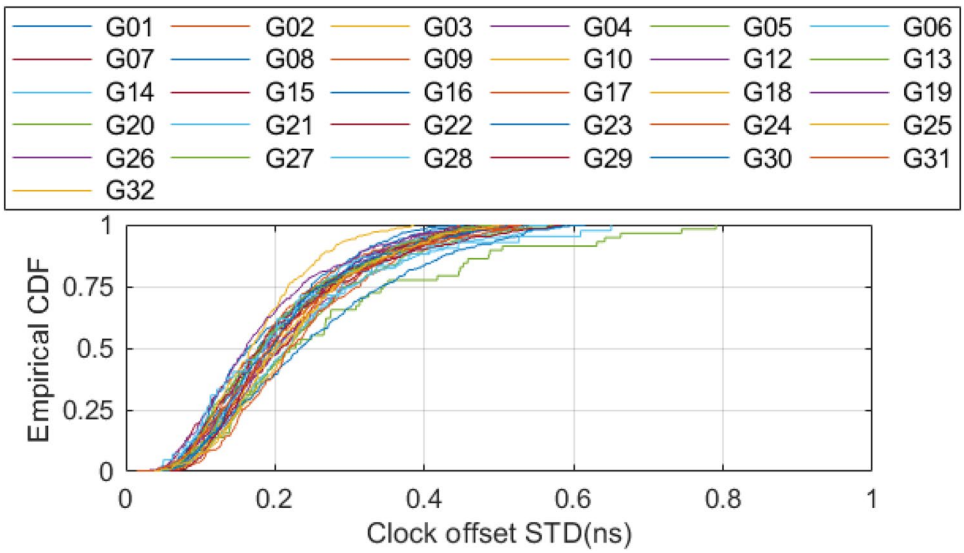

Fig. 11 CDF of GPS satellite clock offset STD

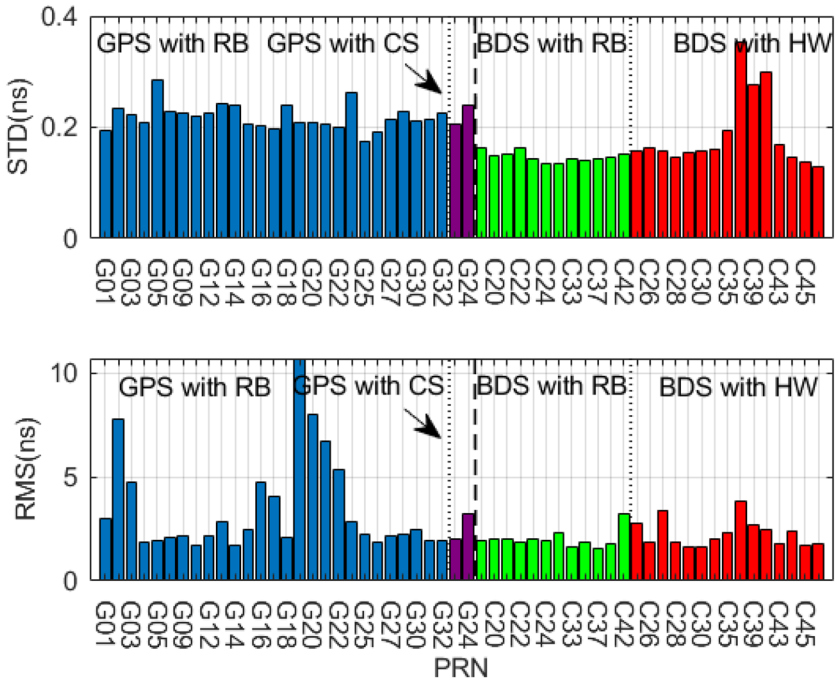

Fig. 12 RMS and STD of each satellite in PPP-B2b, and the upper and lower parts represent STD and RMS, respectively. Different types of clocks are represented with different colors

the daily SISRE STD statistics for the GPS and BDS-3 satellites during the experimental period. The STD of SISRE for BDS-3 IGSO satellites is significantly larger than that of MEO satellites, with the median STD of C38 approaching 0.2 m. The median STD of SISRE for the GPS satellites is close to 0.1 m, while the maximum daily average STD is up to 0.27 m for satellite G23. The median STD of the daily SISRE series for BDS-3 MEO satellites is within 0.1 m, with the maximum daily average STD within 0.2 m.

Table 3 shows the average STD and RMS of SISRE for different types of satellites. It can be seen that the average SISRE STD for the BDS-3 IGSO satellites exceeds 0.1 m, while the average STD for the BDS-3 MEO and GPS satellites is within 0.1 m. The RMS of the GPS, BDS-3 MEO and BDS-3 IGSO satellites can reach 1.025 m, 0.652 m and 1.041 m, respectively, due to the effect of the constant bias in the clock offset.

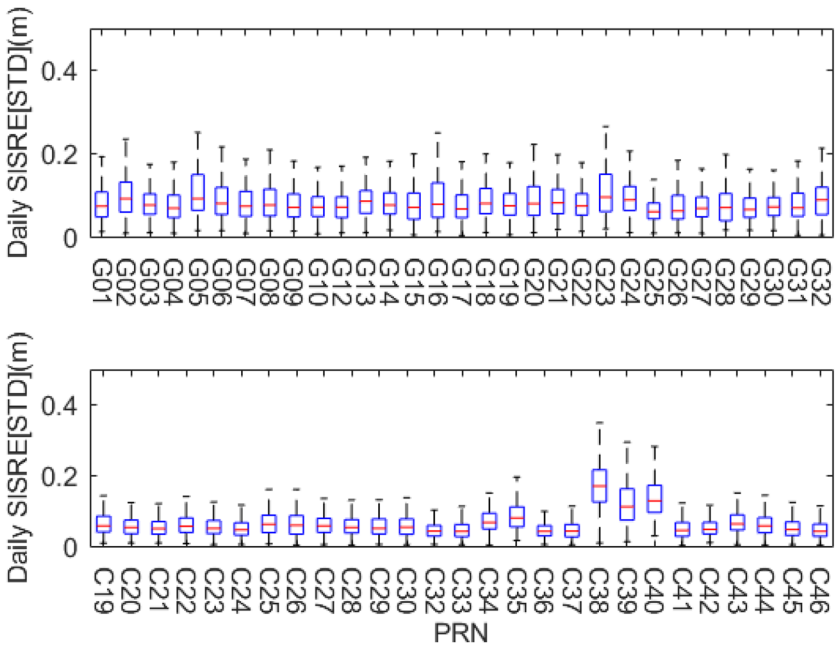

Fig. 13 STD statistics of SISRE for different satellites in PPP-B2b, the upper and lower parts represent GPS and BDS-3, respectively

Table 3 Average RMS and STD of three types of satellites SISRE and SISRE-orbit

System	SISRE-orbit		SISRE	
	STD (m)	RMS (m)	STD (m)	RMS (m)
GPS	0.048	0.106	0.092	1.025
BDS-3 MEO	0.038	0.088	0.059	0.652
BDS-3 IGSO	0.100	0.191	0.174	1.041

PPP experiment

To assess the positioning capability of the PPP-B2b service, a total of 108 days of observations from eleven MGEX stations are selected for the PPP experiment. The station distribution is shown in Fig. 14, and the experiment session is DOY 335 of 2021 to DOY 80 of 2022 (of which the PPP-B2b message is not recorded on DOY 6 of 2022). The detailed PPP strategy is shown in Table 4.

Figures 15 and 16 show the comparison results of static PPP and IGS weekly solutions of JFNG and ULAB stations during the experimental period with three strategies (GPS-only, BDS-3-only and GPS + BDS-3). The north, east and up (NEU) directions are shown in red, green and blue curves, respectively. And the number of available satellites is also shown in the figure. For station JFNG, the STD of daily positioning results are within 0.012 m, 0.028 m and 0.05 m in N, E and U directions for the three strategies, respectively, which instructions the positioning results of PPP-B2b are relatively stable during the experimental period. Furthermore, the average number of available satellites of BDS-3 is significantly more than that of GPS. It is worth noting that since the DOY 55 in 2022, the positioning results of the three stations have improved in the east direction, especially BDS-3, which may be related to the change of PPP-B2b clock estimation strategy, and the specific reasons need further analysis.

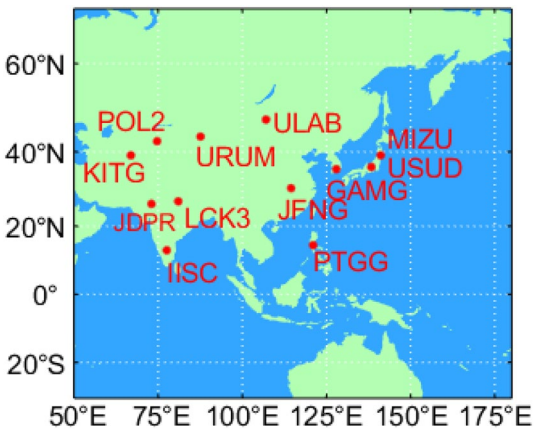

Fig. 14 Distribution of experimental stations

Table 4 PPP solution strategy

Item	Strategy
Orbit/clock offset	CNAV1 + PPP-B2b (BDS-3) LNAV + PPP-B2b (GPS)
Observation	BDS-3: B1/B3 IF combination GPS: L1/L2 IF combination
Observation weight	Code: phase = 1:10,000
Elevation cutoff angle	7°
Ionospheric delay	The first-order ionospheric delay is eliminated by IF combination
Tropospheric delay	Saastamoinen model + random-walk process
Receiver clock	Estimated as white noise for each epoch
Inter-System Biases	Estimated as white noise for each epoch
Ambiguity	Estimated as constant within each arc segment
Estimation	Kalman filter

Figure 17 shows the average positioning accuracy of 12 MGEX stations for 108 days, and the convergence time is defined as the positioning accuracy under 0.1 m in the horizontal direction and 0.2 m in the elevation direction. It can be found that the positioning results of the stations are related to the distribution of the stations. Station POL2, KITG, JDPR, IISC and LCK3 are farther from the center of the PPP-B2b service range, and the positioning accuracy and convergence speed are lower than other stations. For BDS-3, the average RMS of the positioning results of these five stations are 0.028 m,0.052 m and 0.064 m in N, E, and U directions, respectively, and the average convergence time is 54.21 min, which is longer than the average level.

Table 5 lists the average positioning accuracy and the convergence time of stations in the core service area (Xu et al. 2021). The positioning accuracy of GPS-only is 0.025 m, 0.032 m and 0.041 m for north, east and up components, respectively, which is close to that of the IGS RTS service (Hadas et al. 2019). The average convergence time of GPS-only is 50.86 min which is longer than that of BDS-3, probably due to the large constant bias in the clock offset of GPS. The best PPP performance is the GPS + BDS-3 mode with a convergence time of 24.06 min, which improves the convergence time by 35.9% compared to BDS-3-only.

In the static mode, since the position coordinates are treated as constant estimates, some errors have little effect on the position estimation after convergence. The station JFNG, which has better static PPP positioning results, is selected for the kinematic PPP experiment. Figure 18 shows the results of the GPS-only, BDS-3-only and GPS + BDS-3 kinematic PPP on DOY 78 of 2022, with the all-day RMS in the three directions marked with red, blue and green curves, respectively. It can be seen that the GPS-only error

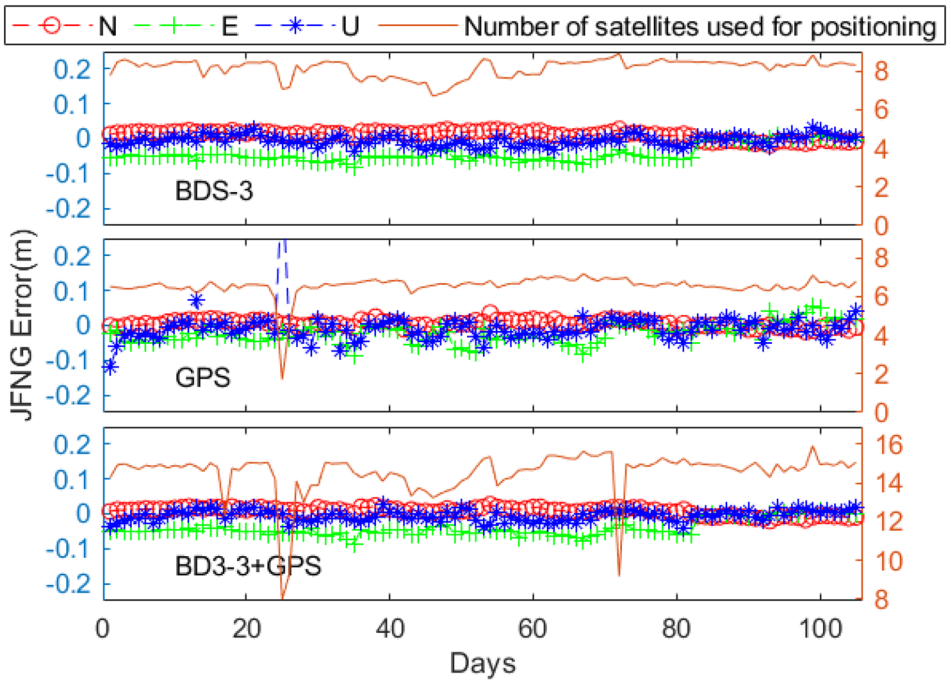

Fig. 15 108-day time series of GPS and BDS-3 single system static PPP results of JFNG. The upper, middle and lower parts of the figure are the results of BDS-3-only, GPS-only and BDS-3 + GPS, respectively

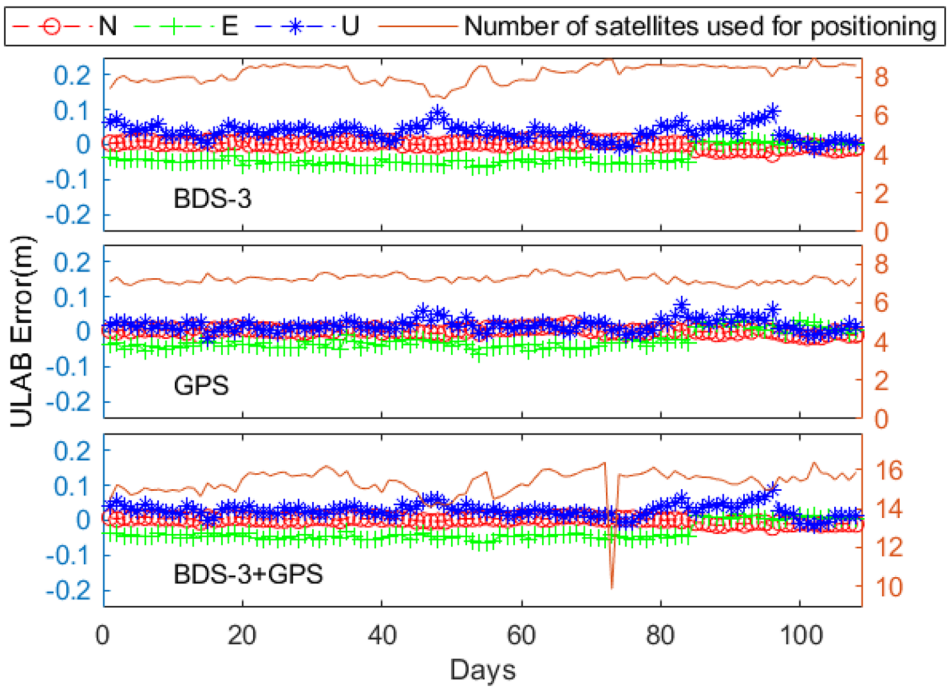

Fig. 16 108-day time series of GPS and BDS-3 single system static PPP results of ULAB. The upper, middle and lower parts of the figure are the results of BDS-3-only, GPS-only and BDS-3 + GPS, respectively

series is significantly larger than that of BDS-3-only and BDS-3 + GPS, especially from 6:00 to 8:00, probably due to the smaller number of available satellites of GPS at this time. The whole day RMS in N, E and U directions could reach 0.078 m, 0.125 m and 0.392 m, respectively, which was significantly higher than that of BDS-3. A similar conclusion can also be drawn from other stations.

Effect of constant satellite-specific clock bias on PPP

Compared to other real-time products, the larger RMS value in the PPP-B2b clock offset means that the constant bias has a more serious impact on PPP, and it is necessary to analyze its impact on the convergence of PPP.

In PPP calculation, since the satellite orbit and clock offset are fixed as known, the constant bias in the clock product

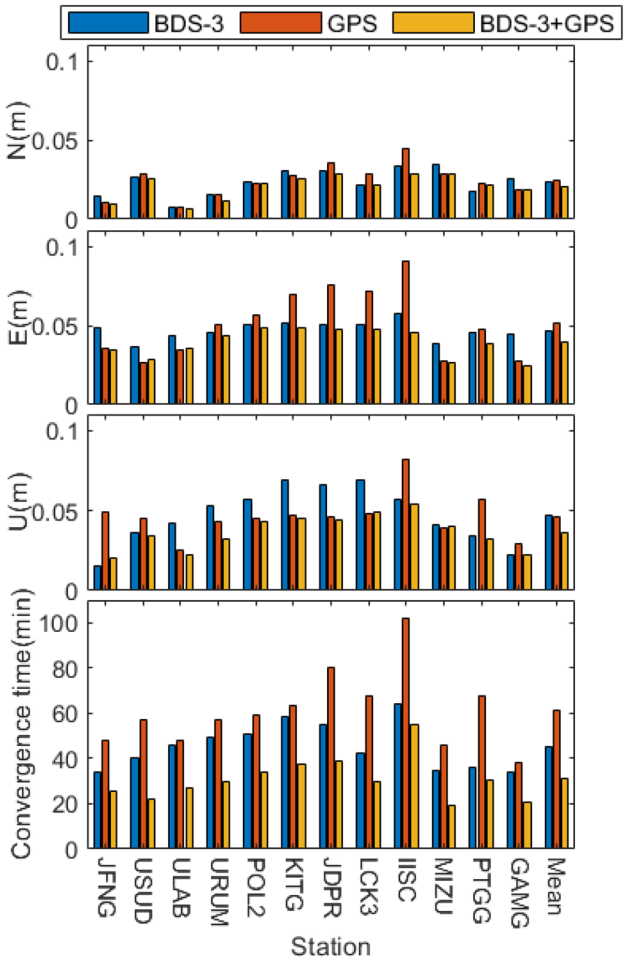

Fig. 17 Static PPP statistical results of different stations. The positioning accuracy in N, E, and U directions and convergence time are shown from top to bottom

Table 5 Positioning accuracy and convergence time of stations in the core service area

	N (m)	E (m)	U (m)	Convergence time (min)
GPS	0.020	0.034	0.041	50.86
BDS-3	0.021	0.043	0.032	37.54
BDS-3 + GPS	0.019	0.032	0.028	24.06

will be absorbed by the pseudorange residual. Therefore, independent parameters related to satellites are added to the pseudorange observation equation to solve the constant deviation. It should be noted that there is a pseudorange bias term related to both receivers and satellites in the pseudorange observation (Gong et al. 2018), and this bias and the clock offset constant bias are combined into the parameter C_r^s (Chen et al. 2022).

$$P_{r,\mathrm{IF}}^s = \rho_r^s + dt_r - dt^s + C_r^s + \delta_{\mathrm{TROP}} + \delta_{P_{\mathrm{IF}}} \tag{9}$$

where C_r^s is the parameter associated with the station and the satellite. ρ_r^s is the geometric distance between receiver and satellite. dt_r and dt^s are the receiver and satellite clock offset. δ_{TROP} is tropospheric delay which can be corrected by model. In addition, the following equation is used to separate the highly correlated dt_r and C_r^s,

$$\sum_{i=1}^{m} C_r^{s_i} = 0 \tag{10}$$

In order to obtain the constant bias in clock offset, the effect of receiver pseudorange bias needs to be eliminated. IGS post-processing products are used to solve the pseudorange bias through (9) (Zhang et al. 2021), and the PPP-B2b clock offset constant bias can be obtained through the following equation:

$$C^s = C_{\mathrm{B2b}}^s - C_{\mathrm{GFZ}}^s \tag{11}$$

where C_{B2b}^s and C_{GFZ}^s are derived with (9) with PPP-B2b and GFZ final products, respectively.

Since the constant bias in PPP-B2b service is different between different arcs, the bias of different satellite arc needs to be re-estimated. Figure 19 shows the results of the BDS-3 satellite constant bias on DOY 325 of 2021. The bias of some satellites can reach 4 ns, and the STD within the same satellite arc is relatively stable, within 0.3 ns.

In order to analyze the impact of clock constant bias, the bias was used as the correction to the clock, and the positioning accuracy was analyzed again. Figure 20 shows the positioning result of station JFNG on DOY 325 of 2021, which is re-initialized every 4 h. The RMS and convergence time of the PPP results for two systems in N, E, U directions within 4 h are counted, and the average value of the results is listed in Table 6. Although the constant bias does not affect the final positioning results, it significantly impacts the positioning results during the convergence phase and the convergence time. For GPS, the RMS of the three directions after correction decreases by 65.7%, 72.0% and 71.0%, respectively, and the convergence time decreases by 48.7%. For BDS-3, the RMS of the three directions was reduced by 42.6%, 47.9% and 38.6%, respectively, and the convergence time was reduced by 65.9%.

Figure 21 shows the pseudorange residuals of some satellites during the convergence phase. It can be seen that the distribution of pseudorange residuals of the two systems is more concentrated after correcting the bias. According to statistics, the RMS of pseudorange residuals of GPS with and without correction are 1.221 m and 2.332 m, respectively, and 1.053 m and 1.225 m for BDS-3. Although this correction is not feasible for real-time usage and only act

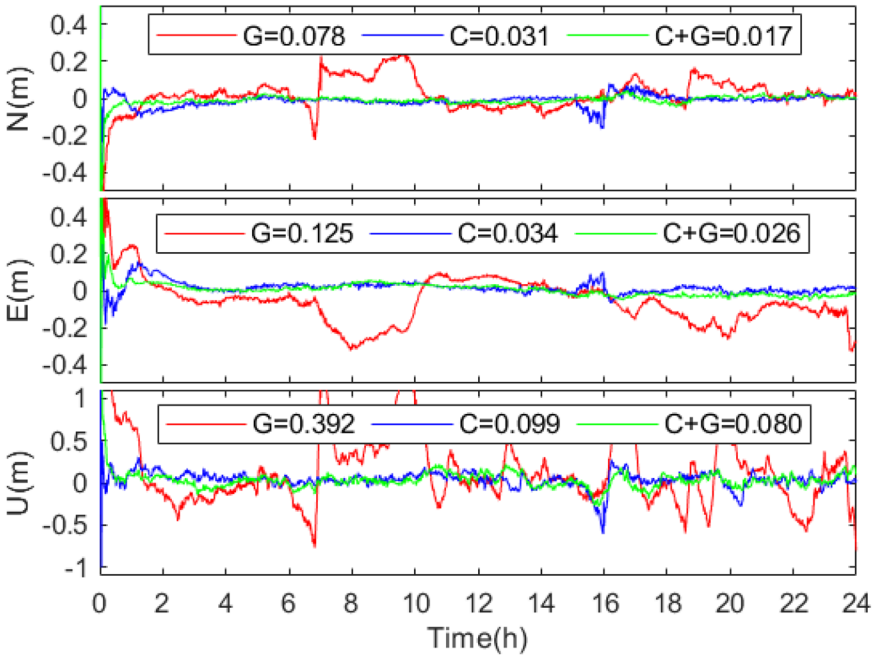

Fig. 18 GPS (red), BDS-3 (blue) and GPS + BDS-3 (green) kinematic PPP sequence, and the average RMS in each direction are shown in the figure

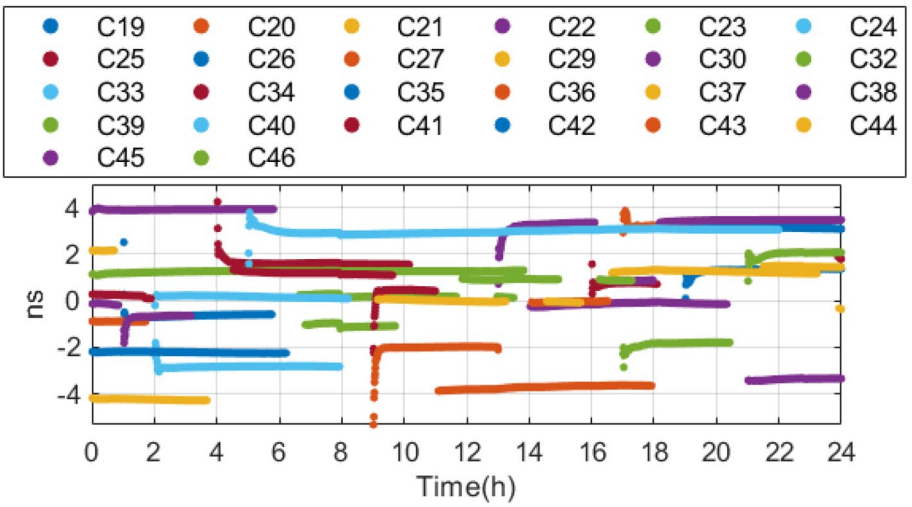

Fig. 19 Constant bias in clock offset of BDS-3

Table 6 Positioning accuracy and convergence time for two strategies

	Without correction				With correction			
	N (m)	E (m)	U (m)	Convergence time (min)	N (m)	E (m)	U (m)	Convergence time (min)
BDS-3	0.136	0.140	0.344	44.3	0.078	0.073	0.194	15.1
GPS	0.297	0.336	0.856	49.9	0.102	0.094	0.248	25.6

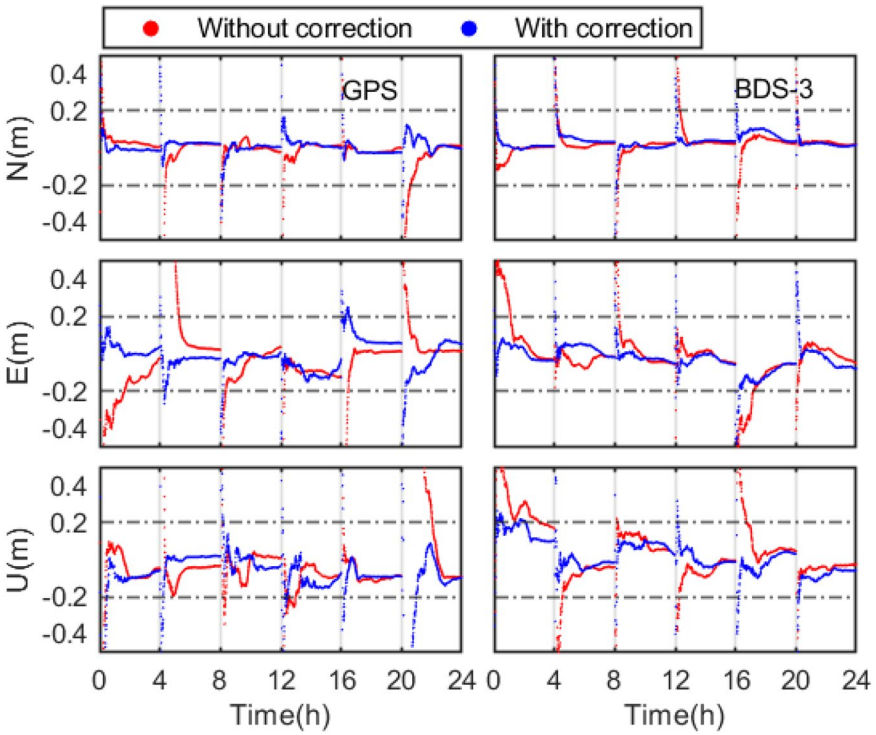

Fig. 20 Positioning results for the two systems with (blue) and without (red) correction strategies. The left and right sides represent GPS and BDS-3, respectively

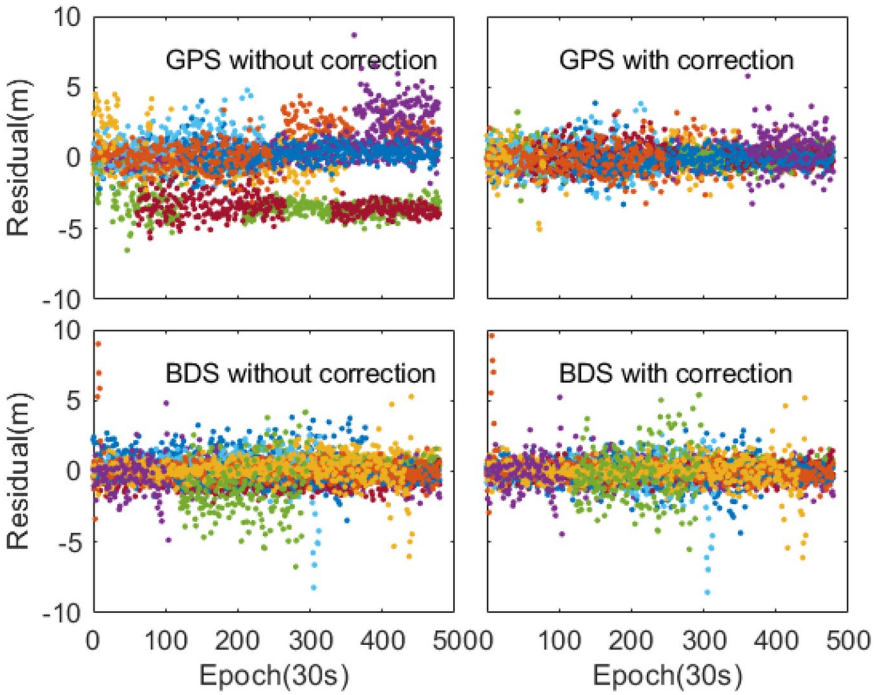

Fig. 21 Pseudorange posterior residual sequence for two strategies, the upper and lower parts represent GPS and BDS-3, respectively

as an analysis manner, it is concluded that the constant bias in the PPP-B2b clock affects the positioning convergence speed.

Conclusion

This paper analyzes the long-term performance of PPP-B2b over nearly 48 weeks. After a series of analyses, PPP-B2b has been proven to be able to provide long-term accurate and

reliable positioning services, and its positioning accuracy meets the positioning performance indicators specified in BeiDou Navigation Satellite System Open Service Performance Standard (CSNO 2021a, b), and the following conclusions can be drawn:

1. Due to the limitation of the regional network on the service side, the satellite correction in the PPP-B2b service is discontinuous, but at least 7 GPS satellites and 8 BDS-3 satellites are available for positioning at any one time within the service area.
2. The average orbit difference in radial of the BDS-3 MEO, GPS and BDS-3 IGSO satellites are 0.056 m, 0.069 m and 0.172 m, respectively, compared to the GFZ final orbit. The difference for the along-track and cross-track is three times or more than the radial. Affected by the ISL observation, the along-track error of BDS-3 satellites is less than the cross-track, while the GPS is on the contrary.
3. Influenced by factors such as pseudorange accuracy at the initial stage of the arc segment, the evaluation method of weighting by arc length is used to evaluate the clock, and the clock offset STD is within 0.2 ns for BDS-3 MEO satellites, 0.25 ns for GPS satellites, and up to 0.3 ns or more for BDS-3 IGSO satellites. The average STD of SISRE of BDS-3 MEO, GPS and BDS-3 IGSO satellites are 0.059 m, 0.092 m and 0.174 m, respectively. The average RMS of SISRE is larger due to the constant bias of the clock offset.
4. The static PPP performance of PPP-B2b is stable and the positioning accuracy can achieve centimeter-level for GPS-only, BDS-3-only and BDS-3 + GPS mode with the convergence time being 61.65 min, 45.12 min and 31.04 min, respectively. The positioning accuracy and convergence time are affected by the distribution of stations. Kinematic PPP results show that the positioning result of GPS-only is worse than that of BDS-3-only.
5. The influence of constant bias in clock offset on PPP is analyzed. The results show that after correcting the bias, The convergence time of GPS and BDS-3 was reduced by 48.7% and 65.9%, respectively. The processing strategy of the bias in PPP-B2b requires further research.

Supplementary Information The online version contains supplementary material available at https://doi.org/10.1007/s10291-023-01409-5.

Acknowledgements The authors thank MGEX for offering observation data, precise satellite orbit and clock, and ILRS for providing SLR data.

Author contributions Author S.S and M.W designed the research; X.M provided the software; S.S and R.J analyzed the result; S.S, M.W and C.L wrote the main manuscript text; All authors reviewed the manuscript.

Data availability The BDS-3 CNAV1 broadcast ephemeris files are downloaded from the website of Test and Assessment Research Center of China Satellite Navigation Office (ftp://ftp2.csno-tarc.cn/cnav). And the LNAV ephemeris for GPS and the GFZ final product are downloaded from the Wuhan University Data Centre of IGS (ftp://igs.gnsswhu.cn/). All the MGEX observation data can be accessed from ftp://igs.gnsswhu.cn//pub/gps/data/daily/.

Declarations

Competing interests The authors declare no competing interests.

References

Borio, D., T. Senni and I. Fernandez-Hernandez (2020). Experimental Analysis of a Candidate Galileo E6-B Data Dissemination Scheme.In: Proceedings of ION ITM 2020, Institute of Navigation, San Diego, California, Jan 21–24, pp 509–520.

Chen G, Wei N, Li M, Zhao Q, Zhang J (2022) BDS-3 and GPS/Galileo integrated PPP using broadcast ephemerides. GPS Solut. https://doi.org/10.1007/s10291-022-01311-6

CSNO (2020). BeiDou Navigation Satellite System Signal In Space Interface Control Document Precise Point Positioning Service Signal PPP-B2b (Version 1.0). http://www.beidou.gov.cn/xt/gfxz/202008/P020200803362062482940.pdf

CSNO (2021) BeiDou Navigation Satellite System Open Service Performance Standard (Version 3.0). http://www.beidou.gov.cn/xt/gfxz/202105/P020210526216231136238.pdf

Dai et al., 2016 Dai L, Chen Y, Lie A, Zeitzew M, Yuki Z (2016) StarFire™ SF3: worldwide centimeter-accurate real time GNSS positioning. In: Proceedings of ION GNSS 2016, Institute of Navigation, Portland, Oregon, USA, Sept 12–16, pp 3295–3320

Gong X, Lou Y, Zheng F, Gu S, Shi C, Liu J, Jing G (2018) Evaluation and calibration of BeiDou receiver-related pseudorange biases. GPS Solut 22(4):98. https://doi.org/10.1007/s10291-018-0765-3

Guo W, Zuo H, Mao F, Chen J, Gong X, Gu S, Liu J (2022) On the satellite clock datum stability of RT-PPP product and its application in one-way timing and time synchronization. J Geod. https://doi.org/10.1007/s00190-022-01638-5

Hadas T, Bosy J (2014) IGS RTS precise orbits and clocks verification and quality degradation over time. GPS Solut 19(1):93–105. https://doi.org/10.1007/s10291-014-0369-5

Hadas T, Kazmierski K, Sośnica K (2019) Performance of Galileo-only dual-frequency absolute positioning using the fully serviceable Galileo constellation. GPS Solut. https://doi.org/10.1007/s10291-019-0900-9

Kazmierski K, Zajdel R, Sośnica K (2020) Evolution of orbit and clock quality for real-time multi-GNSS solutions. GPS Solut. https://doi.org/10.1007/s10291-020-01026-6

Leandro R et al (2011) RTX positioning: the next generation of cm-accurate real-time GNSS positioning. In: Proceedings of ION GNSS 2011, Institute of Navigation, Portland, Oregon, USA, Sept 20–23

Liu C et al (2020) Design and implementation of a BDS precise point positioning service. Navigation 67(4):875–891. https://doi.org/10.1002/navi.392

Liu Y, Yang C, Zhang M (2022) Comprehensive analyses of PPP-B2b performance in China and surrounding areas. Remote Sens. https://doi.org/10.3390/rs14030643

Lu X, Chen L, Shen N, Wang L, Jiao Z, Chen R (2021) Decoding PPP corrections from BDS B2b signals using a software-defined receiver: an initial performance evaluation. IEEE Sens J 21(6):7871–7883. https://doi.org/10.1109/jsen.2020.3041486

Malys S, Jensen PA (1990) Geodetic point positioning with gps carrier beat phase data from the CASA UNO experiment. Geophys Res Lett 17(5):651–654

Montenbruck O, Steigenberger P, Hauschild A (2014) Broadcast versus precise ephemerides: a multi-GNSS perspective. GPS Solut 19(2):321–333. https://doi.org/10.1007/s10291-014-0390-8

Montenbruck O, Steigenberger P, Hauschild A (2018) Multi-GNSS signal-in-space range error assessment—Methodology and results. Adv Space Res 61(12):3020–3038. https://doi.org/10.1016/j.asr.2018.03.041

Montenbruck O et al (2017) The multi-GNSS experiment (MGEX) of the international GNSS Service (IGS)—achievements, prospects and challenges. Adv Space Res 59(7):1671–1697. https://doi.org/10.1016/j.asr.2017.01.011

Nie Z, Liu F, Gao Y (2019) Real-time precise point positioning with a low-cost dual-frequency GNSS device. GPS Solut. https://doi.org/10.1007/s10291-019-0922-3

Nie Z, Wang B, Wang Z, He K (2020) An offshore real-time precise point positioning technique based on a single set of BeiDou short-message communication devices. J Geod. https://doi.org/10.1007/s00190-020-01411-6

Ren Z, Gong H, Peng J, Tang C, Huang X, Sun G (2021) Performance assessment of real-time precise point positioning using BDS PPP-B2b service signal. Adv Space Res 68(8):3242–3254. https://doi.org/10.1016/j.asr.2021.06.006

Sośnica K, Zajdel R, Bury G, Bosy J, Moore M, Masoumi S (2020) Quality assessment of experimental IGS multi-GNSS combined orbits. GPS Solut. https://doi.org/10.1007/s10291-020-0965-5

Tang C, Hu X, Chen J, Liu L, Zhou S, Guo R, Li X, He F, Liu J, Yang J (2022) Orbit determination, clock estimation and performance evaluation of BDS-3 PPP-B2b service. J Geod. https://doi.org/10.1007/s00190-022-01642-9

Tang C et al (2018) Initial results of centralized autonomous orbit determination of the new-generation BDS satellites with inter-satellite link measurements. J Geod 92(10):1155–1169. https://doi.org/10.1007/s00190-018-1113-7

Tao J, Liu J, Hu Z, Zhao Q, Chen G, Ju B (2021) Initial Assessment of the BDS-3 PPP-B2b RTS compared with the CNES RTS. GPS Solut 25(4):131. https://doi.org/10.1007/s10291-021-01168-1

Xu Y, Yang Y, Li J (2021) Performance evaluation of BDS-3 PPP-B2b precise point positioning service. GPS Solut 25(4):142. https://doi.org/10.1007/s10291-021-01175-2

Yao Y, He Y, Yi W, Song W, Cao C, Chen M (2017) Method for evaluating real-time GNSS satellite clock offset products. GPS Solut 21(4):1417–1425. https://doi.org/10.1007/s10291-017-0619-4

Zajdel R, Steigenberger P, Montenbruck O (2022) On the potential contribution of BeiDou-3 to the realization of the terrestrial reference frame scale. GPS Solut. https://doi.org/10.1007/s10291-022-01298-0

Zhang L, Yang H, Gao Y, Yao Y, Xu C (2018) Evaluation and analysis of real-time precise orbits and clocks products from different IGS analysis centers. Adv Space Res 61(12):2942–2954. https://doi.org/10.1016/j.asr.2018.03.029

Zhang W, Lou Y, Song W, Sun W, Zou X, Gong X (2022) Initial assessment of BDS-3 precise point positioning service on GEO B2b signal. Adv Space Res 69(1):690–700. https://doi.org/10.1016/j.asr.2021.09.006

Zhang Y, Kubo N, Chen J, Wang A (2021) Calibration and analysis of BDS receiver-dependent code biases. J Geod 95(4):43. https://doi.org/10.1007/s00190-021-01497-6

Zumberge JF, Heflin MB, Jefferson DC, Watkins MM, Webb FH (1997) Precise point positioning for the efficient and robust analysis of GPS data from large networks. J Geophys Res Solid Earth 102(B3):5005–5017. https://doi.org/10.1029/96jb03860

Shuang Sun received his B.Sc. degree at PLA Strategic Support Force Information Engineering University in 2020, where he is now a Master's degree candidate. His research focuses on GNSS data processing.

Min Wang received his PhD at PLA Strategic Support Force Information Engineering University in 2016 and is an associate professor from PLA Strategic Support Force Information Engineering University. His research is focused on GNSS data processing algorithms.

Changjian Liu received his PhD at PLA Strategic Support Force Information Engineering University in 2011 and is a professor at PLA Strategic Support Force Information Engineering University. His research is focused on error theory and GNSS data processing.

Xin Meng is currently a Master's degree candidate at PLA Strategic Support Force Information Engineering University. He has completed his B.Sc. at the Department of Mining Engineering at Lyuliang University in 2020. His area of research currently focuses on GNSS real-time precise positioning and timing.

Rui Ji obtained his B.Sc degree from PLA Strategic Support Force Information Engineering University, China, in 2016, where he is now a Master's degree candidate. His current research focused on Precise Point Positioning.